

RESEARCH

Open Access



# Discovery of *Cortinarius* O-methyltransferases for the heterologous production of dermolutein and physcion

Pradhuman Jetha<sup>1</sup> , Dominik Mojzita<sup>1</sup> , Natalia Maiorova<sup>1</sup> , Jorg C. de Ruijter<sup>1</sup> , Hannu Maaheimo<sup>1</sup> , Satu Hilditch<sup>1</sup> , Gopal Peddinti<sup>1</sup> , Sandra Castillo<sup>1</sup> , Mervi Toivari<sup>1</sup> , Merja Penttilä<sup>1\*</sup> and István Molnár<sup>1\*</sup>

## Abstract

**Background** Anthraquinones in the emodin family are produced by bacteria, fungi, and plants. They display various biological activities exploited, e.g., for crop protection, and may also be utilized as sustainable, bio-based colorants for the textile, paints, electronics, and cosmetic industries. Anthraquinone pigments from *Cortinarius* mushrooms have been used for artisan dyeing because they are stable, colorfast, and compatible with various dyeing methods. However, their chemical synthesis is complex and uneconomical, and harvesting wild mushrooms from forests in commercial quantities is not feasible.

**Results** Here, we use genomics, transcriptomics, and synthetic biology to uncover the biosynthesis of the anthraquinone scaffold compounds emodin and endocrocin, and their methylation to the yellow pigments physcion and dermolutein in *Cortinarius semisanguineus* and *C. sp. KIS-3*. Both the nonreducing polyketide synthases (nrPKSs), and the regiospecific, fastidious O-methyltransferases (OMTs) are non-orthologous to their Ascomycete counterparts, suggesting a parallel evolutionary origin for the pathway in Basidiomycetes. The genes for the nrPKS and the OMTs are not all clustered in *Cortinarius*, revealing metabolic crosstalk among paralogous nrPKS biosynthetic gene clusters.

**Conclusions** Heterologous biosynthesis of physcion and dermolutein in *Saccharomyces cerevisiae* opens the way to produce specific *Cortinarius* anthraquinones, and to modify these scaffolds to tune their chemistry towards their various applications.

**Keywords** Anthraquinones, *Cortinarius*, Polyketide, Biosynthesis, O-Methyltransferase

## Introduction

O-Methyltransferases (OMTs) represent the largest class of natural product methyltransferases [1]. These enzymes transfer methyl groups from S-adenosylmethionine (SAM) to alcohol or carboxyl functionalities of the substrates to produce their methyl ether or methyl

ester derivatives, respectively [2]. The resulting modification increases the lipophilicity and thus the membrane permeability of the target molecules, modulating their biological activities. Consequently, O-methylation is a widely utilized modification of small molecule drugs in the pharmaceutical industries to improve drug stability, bioavailability, and specificity to interact with the target receptors [3]. Chemical synthetic methods for O-methylation use toxic reagents, and rely on expensive multistep protection/deprotection strategies to achieve regiospecificity. They are also prone to unwanted side reactions [3], posing economic and sustainability challenges when applied on an industrial

\*Correspondence:

Merja Penttilä  
merja.penttila@vtt.fi  
István Molnár  
istvan.molnar@vtt.fi

<sup>1</sup> VTT Technical Research Centre of Finland, Tekniikantie 21, 02150 Espoo, Finland



© The Author(s) 2025. **Open Access** This article is licensed under a Creative Commons Attribution-NonCommercial-NoDerivatives 4.0 International License, which permits any non-commercial use, sharing, distribution and reproduction in any medium or format, as long as you give appropriate credit to the original author(s) and the source, provide a link to the Creative Commons licence, and indicate if you modified the licensed material. You do not have permission under this licence to share adapted material derived from this article or parts of it. The images or other third party material in this article are included in the article's Creative Commons licence, unless indicated otherwise in a credit line to the material. If material is not included in the article's Creative Commons licence and your intended use is not permitted by statutory regulation or exceeds the permitted use, you will need to obtain permission directly from the copyright holder. To view a copy of this licence, visit <http://creativecommons.org/licenses/by-nc-nd/4.0/>.

scale. To achieve the required specificity and regioselectivity for the *O*-methylation of highly complex and reactive scaffolds, the development of more specific and environmentally benign approaches remains a high priority [1].

As opposed to chemical synthesis, enzymatic *O*-methylation proceeds with a high yield under mild, environmentally friendly reaction conditions and offers regio- and stereospecific outcomes [3]. Moreover, the substrate promiscuity and regioselectivity, and the process parameters of the enzymes may be altered by various protein engineering approaches. For example, the regioselectivity of resorcylic acid lactone *O*-methyltransferases has been modulated by structure-guided site-directed mutagenesis [3], while catechol *O*-methyltransferase variants have been exploited to transfer alkyl groups regio-selectively to the important clinical drug rapamycin, thus generating new lead compounds [1]. However, the high cost of the methyl donor co-substrate SAM and its inefficient regeneration limits the scalability and thus the industrial applicability of in vitro reaction systems [3]. Instead, the biotechnology industries employ in vivo biocatalytic or total biosynthetic platforms to

produce *O*-methylated small molecules as the cells synthesize and recycle SAM efficiently.

Anthraquinones (AQ) are an important class of polyketide natural products with a wide applicability in the textiles, food, cosmetics, paints, electronics, pharmaceutical, and crop protection industries [4, 5]. Emodin (1) and endocrocin (2, Fig. 1) are common biosynthetic intermediates of the AQs as well as the benzophenones, diphenyl ethers, xanthenes and other members of the “emodin family” of compounds, produced by many plants, bacteria and fungi [6]. Emodin and endocrocin are derived from the octaketide atrochrysonic acid (3), the first enzyme-free intermediate released by the polyketide synthase (PKS) enzymes in these organisms. Regio-specific *O*-methylation is a common biosynthetic step to further diversify emodin, endocrocin and their derivatives. Among these, physcion (4), the 6-*O*-methylated derivative of emodin, displays laxative, hepatoprotective, antitumor, and anti-inflammatory activities [7]. It is also the active ingredient of a commercially approved fungicide used to treat powdery mildew infections in plants [8]. Industrial-scale production of physcion (4) relies on extracting the compound from the roots of the Chinese

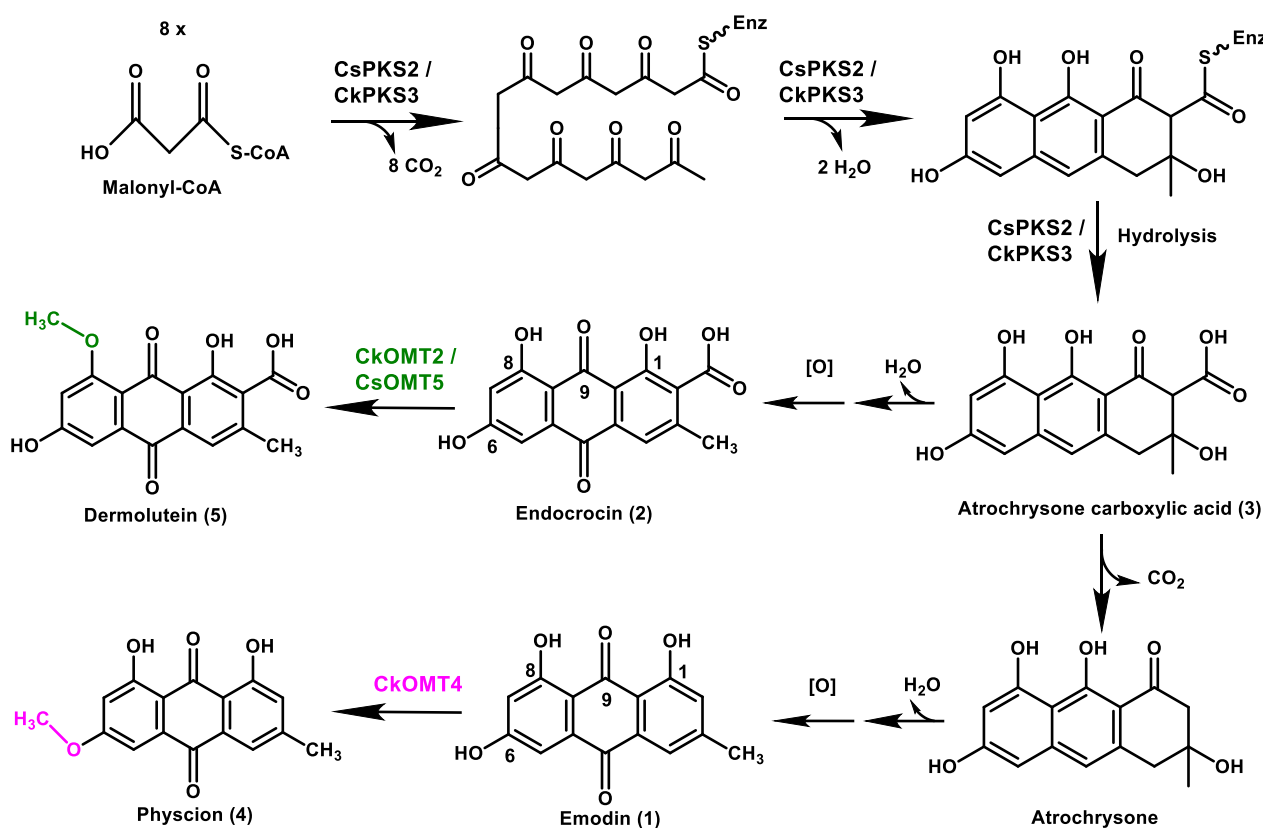


**Fig. 1** Biosynthesis of dermolutein and physcion in *Cortinarius* spp. CkPKS3 (in *Cortinarius* sp. KIS-3) or CsPKS2 (in *C. semisanguineus*) are responsible for the iterative condensation of malonyl-CoA precursors to produce atrochrysonic acid (3) that is then converted to emodin (1) or endocrocin (2). CkOMT4, or CkOMT2 and CsOMT5 *O*-methylate these AQs to afford physcion (4) or dermolutein (5), respectively

rhubarb (*Rheum palmatum*) [9]. However, physcion concentration in these roots reaches only 0.01–0.2% [10], limiting the productivity. To develop biocatalytic routes towards physcion, two recent publications described the identification of *O*-methyltransferases from Ascomycete fungi that can methylate the C6 alcohol of emodin [10, 11]. Two bacterial and a plant-derived OMTs have also been described to catalyze the same conversion to a limited extent [10]. A different OMT from the ascomycete *Aspergillus terreus* has been identified to produce questin (8-*O*-methylemodin), a regioisomer of physcion that displays antimicrobial activities [2, 12].

In contrast to that of emodin, the genetic and enzymatic basis for endocrocin *O*-methylation received little attention. Endocrocin may be *O*-methylated at the 8-OH position to yield dermolutein (5), an AQ with potential applications as a photosensitizer [13], and as a dye for textiles [14] and human hair [15]. This yellow-orange pigment is biosynthesized by the basidiomycete fungi *Cortinarius* spp. in the *Dermocybe* group, as an intermediate towards the characteristic red pigment dermorubin. The same mushrooms also produce emodin-derived yellow (physcion 4) and red pigments (dermoglaucin and dermocycin, both oxidized derivatives of 4), and have been used for artisan yarn dyeing in Finland [14, 16, 17]. Because of their stability, color-fastness, and compatibility with various dyeing methods [14, 16, 17], these pigments have the potential to replace widely used synthetic dyes produced from non-renewable, petrochemical-based sources. However, the abundance of dermolutein (5) and physcion (4) in *Cortinarius* fruiting bodies is low, limiting their production, bioactivity evaluation, and potential applications.

A recent publication revealed that emodin (1) and endocrocin (2) are produced in *C. odorifer* by two orthologous nonreducing PKSs (nrPKSs) with a domain organization different from those in Ascomycetes [18]. These AQ synthases, just as many other basidiomycete nrPKSs [19], lack an SAT (starter acyltransferase) domain for chain initiation with acetyl-CoA, but possess an integrated TE (thioesterase) domain for product release. However, to the best of our knowledge, neither biosynthetic nor chemical synthetic routes have been described up till now to produce dermolutein (5), and the OMT enzyme that yields physcion (4) in *Cortinarius* spp. also remained unknown. In this work, we used genomics, comparative transcriptomics, and synthetic biology to identify orthologous nrPKSs from two *Cortinarius* spp. that afford emodin (1) and endocrocin (2), and to discover distinct OMTs that modify these intermediates to produce their respective *O*-methylated derivatives, physcion (4) and dermolutein (5). Importantly, the nrPKSs yielding emodin (1) and endocrocin

(2), and the OMTs that produce physcion (4) and dermolutein (5) do not all reside in the same biosynthetic gene clusters, revealing metabolic crosstalk and a complex evolutionary history involving gene duplications and cluster diversification. Further, we used *in vivo* biocatalytic conversion and *in vitro* reconstituted reactions with purified OMTs to show that these enzymes are fastidious in their substrate selection. Utilizing AI-assisted protein structure modeling, we also predict structural determinants that may contribute to the distinct regiospecificities of these OMTs. Generating efficient synthetic biology production systems for the *Cortinarius* Aqs would open the way to modify these scaffolds *in vivo* or *in vitro* to tune their properties for the textile, plastics, paints, food, electronics, and cosmetic industries, as well as for crop protection and pharmaceutical applications [4, 5].

## Results and discussion

### Identification of putative AQ biosynthetic gene clusters in *Cortinarius semisanguineus* and *Cortinarius* sp. KIS-3

We have sequenced the genome of *Cortinarius semisanguineus* F-YF12, a prominent AQ producer ectomycorrhizal basidiomycete, using a combination of Illumina and PacBio technologies (Supplementary Information [SI] Table S1). We have also created transcriptomic databases of the colored tissues of the cap and stipe of the mushroom collected in forests in Finland, and the non-colored mycelia that contain only trace amounts of Aqs, grown in a static liquid surface culture in the laboratory. We utilized a comparative genomics and transcriptomics approach to search for the biosynthetic gene cluster (BGC) responsible for AQ pigment production in *C. semisanguineus* and the related AQ producer *Cortinarius* sp. KIS-3 whose genome sequence is available in the JGI MycoCosm database. We identified two orthologous nrPKS candidates encoded in the genome sequence of *C. semisanguineus* (CsPKS1 and 2), and three orthologous nrPKSs in that of *C. sp. KIS-3* (CkPKS3 to 5) that show identical domain organization and > 65% sequence identities to the *C. odorifer* AQ synthases CoPKS1 and CoPKS4 [18] (Fig. 2 and SI Tables S2, S3). The genes for both CsPKS1 and CsPKS2 were found to be highly expressed in the stipe and the cap tissues of *C. semisanguineus* where AQ pigment production is active, while their expression was negligible in the pure culture where AQ production is largely absent (SI Table S4). The three nrPKS-encoding genes of strain KIS-3 were also expressed in the red sporophore tissues, although transcriptomic datasets for AQ-nonproducer mycelia were not available in the JGI MycoCosm database.

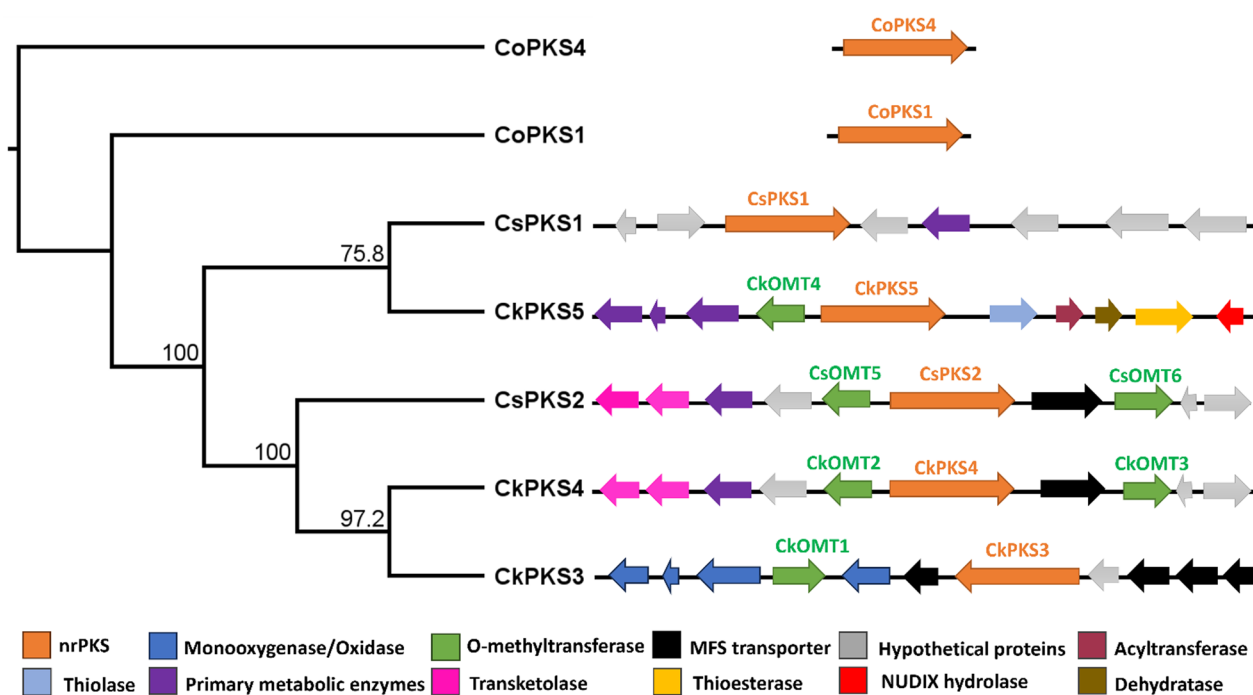


**Fig. 2** Phylogenetic tree and genomic loci of nrPKSs in *C. semisanguineus* and *C. sp.* KIS-3 that are orthologous to the *C. odorifer* AQ synthase CoPKS1 and CoPKS4 [18]. The evolutionary history of the tree was inferred using the neighbor-joining method with a bootstrap test of 1000. See SI Tables S5–S9 for annotations of the predicted genes. MFS, major facilitator superfamily

### Validation of CsPKS2 and CkPKS3 as AQ synthases

Considering that no genetic tools are available for *Cortinarius* spp., we relied on heterologous expression in *Saccharomyces cerevisiae* to functionally identify the nrPKS-encoding genes of *C. semisanguineus* and *C. sp.* KIS-3. First, the genes encoding the phosphopantetheinyl transferase NpgA [20, 21] (essential for PKS activity) and the allosterically insensitive acetyl-CoA carboxylase double mutant ACC1<sup>S659A,S1157A</sup> (to increase the supply of the AQ precursor malonyl-CoA) were integrated into the *LEU* locus of *S. cerevisiae* H4590 to construct strain H6108 (SI Table S10). Next, we separately integrated codon-optimized, intronless, custom-synthetic genes for CsPKS1, CkPKS3, and CkPKS4, and the cDNA-derived open reading frame of CsPKS2 into the *HIS* locus of *S. cerevisiae* H6108, under the control of a synthetic expression system (SES) [22]. Since gene synthesis for CkPKS5 failed despite multiple attempts, and neither genomic DNA nor mRNA was available to us from *C. sp.* KIS-3, the function of this nrPKS remains unidentified. Expression of the genes for CsPKS1 and CkPKS4 did not yield any new metabolites in the *S. cerevisiae* chassis. However, *S. cerevisiae* strains expressing CsPKS2 or CkPKS3 both produced emodin (1) associated with the cells (0.25 mg/L), and endocrocin (2) localized in the culture supernatant (1.25 mg/L) (Fig. 3).

### Identification of regiospecific *Cortinarius* OMTs that modify emodin (1) and endocrocin (2)

To further characterize the bifurcating *Cortinarius* AQ biosynthetic pathway from emodin (1) to physcion (4) on one branch, and endocrocin (2) to dermolutein (5) on the other (Fig. 1), the putative OMTs encoded in the selected nrPKS genomic loci of *C. semisanguineus* and *C. sp.* KIS-3 (Fig. 2 and SI Table S11) were investigated next. For this, we considered both total biosynthesis (i.e., production of the individual OMTs in a chassis that biosynthesizes the polyketide substrates emodin and endocrocin) and biocatalytic platforms (i.e., supplementing emodin or endocrocin to cultures of chassis strains producing the individual OMTs only). *S. cerevisiae* H6108 strains co-expressing the gene for CkPKS3 with those for any of CkOMT1, CkOMT3, or CsOMT6, respectively, did not yield any methylated AQ derivatives, thus these OMTs were not investigated further. In contrast, the yeast strain that co-expressed CkPKS3 with CkOMT4 (derived from the CkPKS5 BGC of *C. sp.* KIS-3) afforded physcion (4) in addition to the PKS-produced emodin (1) and endocrocin (2, Fig. 3). Similarly, *S. cerevisiae* H6108 producing only CkOMT4 successfully *O*-methylated commercial emodin (1) at the 6-OH position to yield physcion (4, Fig. 4A). However, the yeast strain producing this OMT did not afford methylated derivatives of endocrocin (2), nor were *O*-methylated endocrocin derivatives obtained

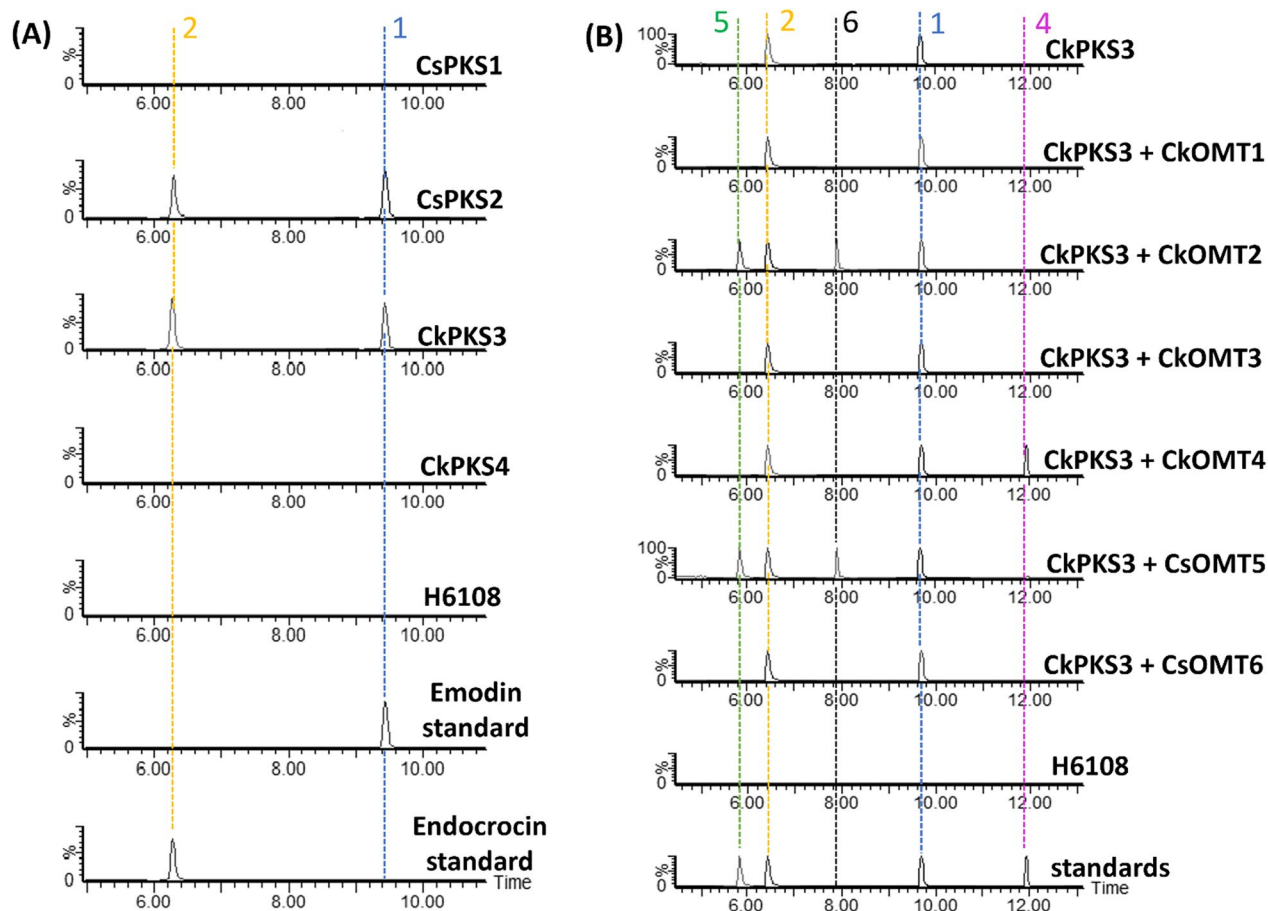


**Fig. 3** Total biosynthesis of emodin (1), endocrocin (2) and their *O*-methylated derivatives in *S. cerevisiae*. Product profiles (HRMS ion chromatograms with the extracted *m/z* values of compounds **1**, **2**, **4**, **5** and **6**) from cultures of *S. cerevisiae* H6108 strains that: **(A)** express the genes for the selected nrPKSs of *C. semisanguineus* or *C. sp. KIS-3*; or **(B)** co-express the genes for CkPKS3 and the selected OMTs of *C. semisanguineus* or *C. sp. KIS-3*. The trace at the bottom of Panel B represents the overlay of extracted ion chromatograms for: authentic emodin (**1**), endocrocin (**2**), physcion (**4**), and dermolutein (**5**) standards. Culture extracts of the *S. cerevisiae* H6108 chassis are also shown in both panels. The extracted ion chromatograms (EICs) are *m/z* 269.044 [M-H]<sup>-</sup> for (**1**); 313.038 [M-H]<sup>-</sup> for (**2**); 283.062 [M-H]<sup>-</sup> for physcion (**4**); 327.046 [M-H]<sup>-</sup> for dermolutein (**5**); and 283.062 [M-H]<sup>-</sup> for an uncharacterized *O*-methylmodin (**6**), possibly questin (8-*O*-methylmodin; a questin standard was not available and the yield of the metabolite was too low for isolation and structure elucidation)

by total biosynthesis in the strain that produces both CkPKS3 and CkOMT4 (Figs. 3 and 4B).

Strains co-producing CkPKS3 with either CkOMT2 (encoded in the CkPKS4 BGC of *C. sp. KIS-3*) or CsOMT5 (from the *C. semisanguineus* CsPKS2 BGC) afforded dermolutein (**5**) by *O*-methylating the PKS-generated endocrocin (**2**) at the 8-OH group (Fig. 3B). Strains producing either CkOMT2 or CsOMT5 also yielded dermolutein (**5**) upon biocatalytic conversion of endocrocin (**2**) supplemented to the cultures (Fig. 4B). Small amounts of a methylated emodin derivative (**6**) with a chromatographic mobility different from that of physcion, likely questin (8-*O*-methylmodin), were also produced by these OMTs in both biocatalytic or total biosynthetic formats (Figs. 3 and 4A), but the structure of

this product could not be elucidated due to its low yield. Compounds **4** and **5** were produced and isolated from upscaled fermentations and their structures were validated (physcion **4** [23], SI Table S12.1 and SI Figs. S1–S5), or elucidated (dermolutein **5**, SI Table S12.2 and SI Figs. S6–S10) by analyzing their 1D and 2D NMR spectra, and LC–MS/MS data.

To understand the evolutionary relationships of the *Cortinarius* OMTs, a phylogenetic tree (Fig. 5), was constructed based on a multiple sequence alignment with recently identified OMTs (SI Table S13) affording physcion [10, 11] and questin [2]. Although the *Cortinarius* OMTs yield AQ products with distinct regioselectivity, they form a single, strongly supported clade. This clade is sister to that of GedA, a class II

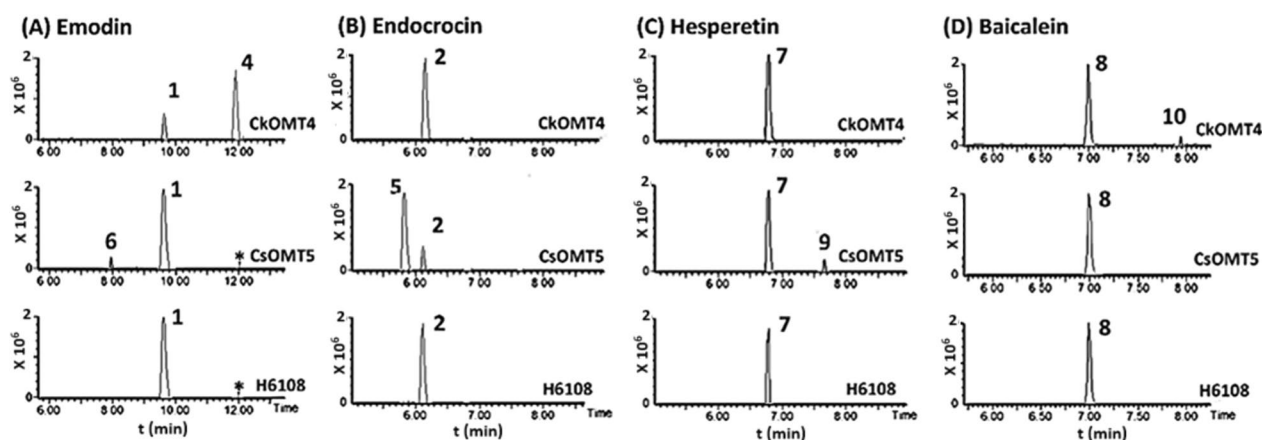


**Fig. 4** Substrate selectivities of CkOMT4 and CsOMT5. Product profiles (HRMS ion chromatograms with the extracted  $m/z$  values of the substrates and their methylated derivatives) from in vivo biocatalytic reactions with *S. cerevisiae* H6108 expressing the genes for CkOMT4 or CsOMT5, supplemented with the substrates: **(A)** emodin **(1)**; **(B)** endocrocin **(2)**; **(C)** hesperetin **(7)**; or **(D)** baicalein **(8)**. Control biocatalytic reactions with the yeast chassis are also shown. \*, commercial emodin contains minor amounts of physcion **(4)** as an impurity. The extracted ion chromatograms (EICs) are  $m/z$  269.044 [M-H]<sup>-</sup> for **(1)**; 313.038 [M-H]<sup>-</sup> for **(2)**; 283.062 [M-H]<sup>-</sup> for physcion **(4)**; 327.046 [M-H]<sup>-</sup> for dermolutein **(5)**; 283.062 [M-H]<sup>-</sup> for the uncharacterized *O*-methylemodin **(6)**; 301.07 [M-H]<sup>-</sup> for hesperetin **(7)**; 269.044 [M-H]<sup>-</sup> for baicalein **(8)**; 315.09 [M-H]<sup>-</sup> for the putative *O*-methylhesperetin **(9)**; and 283.062 [M-H]<sup>-</sup> for the putative *O*-methylbaicalein **(10)**.

emodin-*O*-methyltransferase that produces questin (8-*O*-methylemodin) in *Aspergillus terreus* [2]. Nevertheless, the *Cortinarius* AQ OMTs that show different regioselectivities share less than 40% identity with each other (SI Table S14, SI Fig. S11), and are at most 30% identical to GedA (SI Table S15). Their sequence similarities with other known OMTs that are able to methylate emodin are even more tenuous (SI Table S15) and are mostly constrained to the shared Rossmann-fold SAM-binding site, even if they are able to produce the same product (physcion). Thus, parallel evolution utilized the generalized methyltransferase fold to produce multiple, distinct sequence solutions for enzymes that may carry out the *O*-methylation of the widely distributed emodin and endocrocin skeletons in different phylogenetic lineages.

#### Docking models for the *Cortinarius* OMT-SAH-AQ complexes reveal distinct substrate binding poses

We generated AlphaFold2 protein structure models for CkOMT4 and CsOMT5. Despite the low primary sequence identities (SI Table S15 and SI Fig. S11), these structure models aligned well with the recently published crystal structure of GedA (PDB id: 7WH9), the emodin-8-OMT of *A. terreus* [2] (RMSD [root mean square deviation] of 2.65 and 3.44 Å to CkOMT4 and CsOMT5, respectively) (SI Figs. S12, S13, and S14). The co-product *S*-adenosylhomocysteine (SAH) was then docked into the CkOMT4 and CsOMT5 models to reveal highly conserved SAM binding sites, similar to that of GedA [2] (SI Figs. S11 and S12). Thus, aromatic residue W216 (CkOMT4) or W215 (CsOMT5) is predicted to

interact with the adenine moiety of SAH through  $\pi$ - $\pi$  stacking. The ribose moiety of SAH may be stabilized by the canonical DXGGXXG motif [24] along with hydrogen bonds to R337 (CkOMT4) or D288 (CsOMT5). The homocysteine tail of SAH may also establish an extensive hydrogen bonding network with the side chains of R337, K272, and V273 in CkOMT4, while a similar network with SAH may be formed by R336, G267, and N270 in CsOMT5.

Next, the substrates (emodin **1** for CkOMT4 and endocrocin **2** for CsOMT5) were docked into the SAH-OMT complexes (Fig. 6). This revealed conserved active site residues which could contribute to the S<sub>N</sub>2-type nucleophilic reaction, as seen with typical class II OMTs including GedA [2]. Thus, E420 (in CkOMT4) or E404 (in CsOMT5) may serve as an acid to polarize H341 (in CkOMT4) or H340 (in CsOMT5) which then act as a base to deprotonate the 6-OH group of emodin or the 8-OH of endocrocin, respectively. The corresponding phenolate ions of the substrates would then act as nucleophiles to abstract the positively charged methyl group of SAM, giving rise to the *O*-methylated products along with SAH.

In contrast, the predicted substrate binding sites diverge in these OMTs (Fig. 6 and SI Fig. S11), even for CkOMT4 and GedA that share the same substrate (emodin **1**) but produce regioisomeric products (physcion for CkOMT4 and questin for GedA). These distinct substrate binding cavities likely determine the substrate acceptance of CkOMT4 vs. CsOMT5 (emodin vs. endocrocin), and position the substrates for a regioselective *O*-methylation

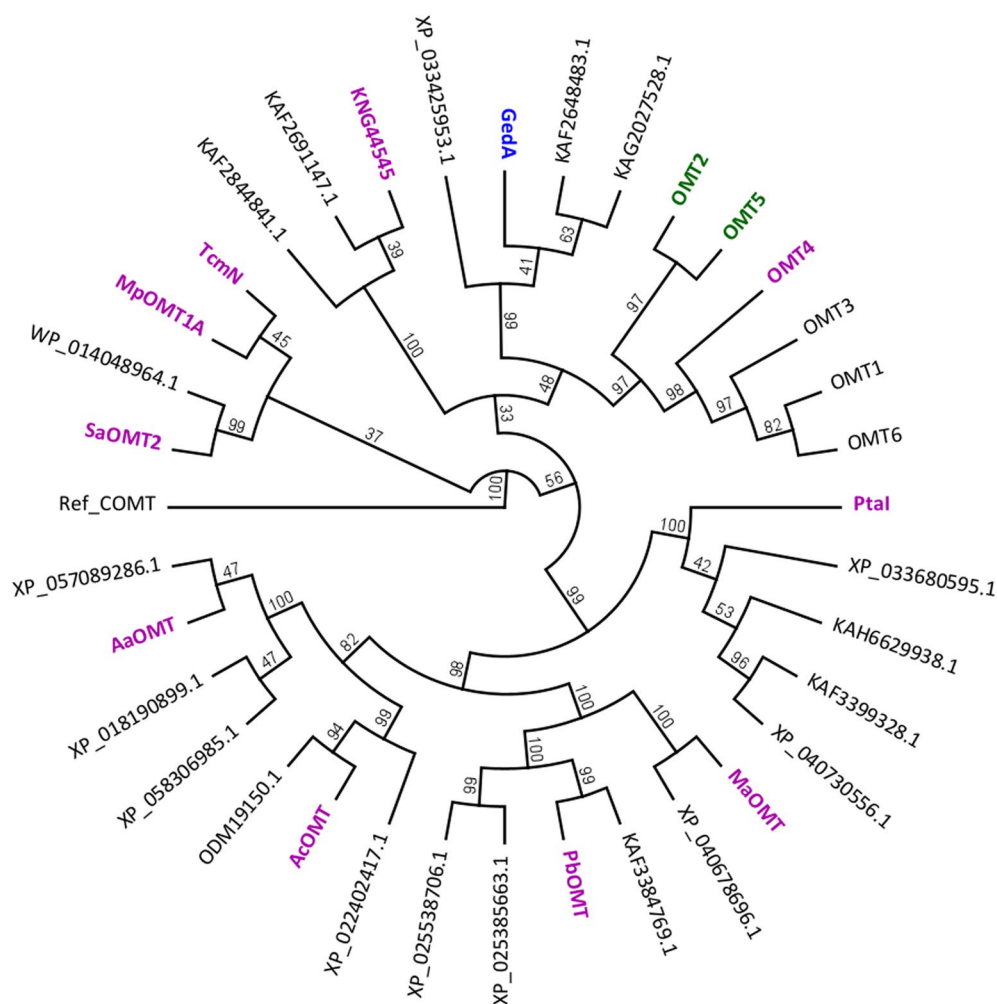


**Fig. 5** Evolutionary relationships of *Cortinarius* OMTs. OMTs yielding dermolutein (8-O-methylendocrocin) are in green; those able to produce phycion (6-O-methylendocrocin) are in pink; those affording quercetin (8-O-methylendocrocin) are in blue; while selected putative OMTs orthologous to these functionally characterized enzymes are shown in black. Note that OMTs able to produce phycion in synthetic biology systems may yield different products when part of their native biosynthetic pathways in their native producer organisms. The evolutionary history of the tree was inferred using the neighbor-joining method with a bootstrap test of 1,000, with the caffeic acid OMT (Ref\_COMT) from *Zea mays* as the outgroup. See SI Table S13 for the GenBank accessions of the sequences

outcome, explaining the observed differences in the substrate selectivities and product regioselectivities of these enzymes. In CkOMT4, emodin is surrounded by F231, F338, and M408 which may contribute hydrophobic and Van der Waals interactions, while similar interactions from residues M235 (M269 in GedA) and M412 (M438 in GedA) may stabilize the horizontal position of the substrate from opposite sides of the aromatic plane. Residue D342 may form a hydrogen bond with the 6-OH group of emodin, orienting this moiety towards the methyl group of SAM for phycion (**4**) formation. In GedA, this phenolic alcohol is engaged in hydrogen bonds with residues R434 and Y173, exposing the 8-OH group for methylation to yield quercetin. However, these GedA residues are

replaced by M408 and F176 in CkOMT4, thus a pose that would orient the 8-OH group towards the activated methyl group of SAM is not favored in the *Cortinarius* enzyme.

Docking endocrocin into the SAH-CsOMT5 complex indicated that the aromatic plane of the substrate is bracketed by H178 and H395 from one side and H340 and D341 from the opposite side. These residue pairs may form hydrogen bonds with the two carbonyl oxygens and stabilize the horizontal position of the substrate. Additionally, the carboxylic acid moiety of endocrocin may establish hydrogen bonds with the R369 side chain, thus prohibiting a 180° rotation of the substrate along to the plane. This would ensure that the C8 instead of the C1

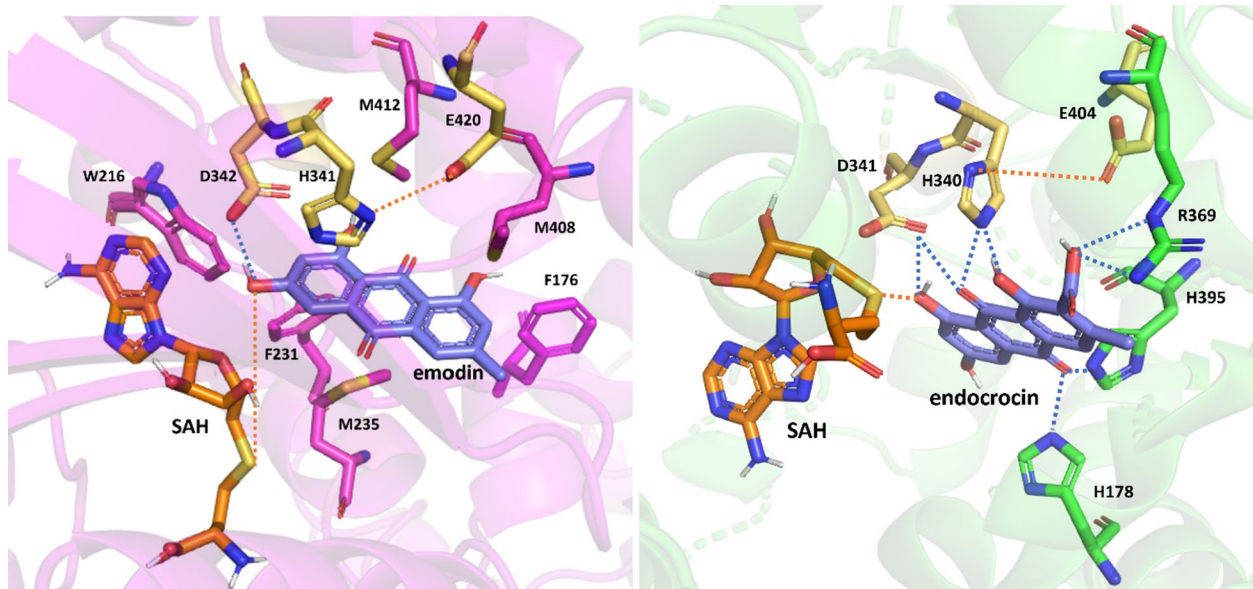


**Fig. 6** Predicted substrate binding sites in CkOMT4 (pink) and CsOMT5 (green). Orange sticks, the co-product *S*-adenosylhomocysteine (SAH); blue sticks, the substrate (emodin **1** for CkOMT4 and endocrocin **2** for CsOMT5); yellow sticks, the predicted catalytic residues; pink and green sticks, the substrate binding sites of CkOMT4 and CsOMT5, respectively. Predicted hydrogen bonds (cyan) and key interactions (orange) are indicated with dashed lines

phenolic alcohol approaches the methyl group of SAM. Meanwhile, D341 may form hydrogen bonds with both the 8-OH and the C9 carbonyl group, breaking the intramolecular hydrogen bond in endocrocin and setting up 8-OH for methylation to yield dermolutein (**5**).

#### Substrate selectivities of the *Cortinarius* AQ OMTs

To explore the substrate promiscuity and combinatorial biosynthetic capacity of the *Cortinarius* OMTs, we challenged these enzymes with various AQ and flavonoid substrate analogues (SI Table S16). First, *S. cerevisiae* strains producing either CkOMT4 or CsOMT5 were used to biotransform these potential substrates supplemented to the cultures. Out of the 13 analogues tested, CsOMT5 accepted only emodin and hesperetin as substrates to yield *O*-methylated derivatives (Fig. 4A, C). However, the conversion efficiencies were very low (<0.2%). CkOMT4 only accepted baicalein as a substrate, but with even less efficiency (Fig. 4D). Because of the poor yields, the *O*-methylated derivatives could not be isolated to determine the regioselectivities of the reactions.

Next, the genes for CkOMT4 and CsOMT5 were expressed in *E. coli* BL21 strain (SI Table S17) to yield *N*-terminally His-tagged proteins, but the enzymes were only produced as inactive inclusion bodies despite our best efforts to optimize expression conditions such as inducer concentrations and expression temperatures. However, *N*-terminally His-tagged CkOMT4 and

CsOMT5 were successfully produced in *S. cerevisiae* H6111 to afford active, soluble proteins that were isolated using Ni-affinity chromatography (SI Fig. S15) [25]. In vitro reactions with the isolated enzymes with the AQ and flavonoid candidate substrates (SI Table S16) revealed methylation of the same substrates (emodin and baicalein with CkOMT4; emodin, endocrocin, and hesperetin with CsOMT5; SI Fig. S16) as in the in vivo biocatalytic reactions (Fig. 4). Docking representative potential substrates into our CkOMT4 or CsOMT5 structure models failed to reveal the reasons for substrate selectivity or product regioselectivity, indicating the need for future structural biology experiments with these interesting enzymes.

#### Conclusions

*Cortinarius* spp. (from the *Dermocybe* subgroup) produce a variety of AQ pigment congeners from the emodin family that provide vivid colors and display various bioactivities that presumably grant an evolutionary advantage to these fungi in their native ecological niche [26, 27]. To produce these Aqs, these Basidiomycetes utilize nrPKSs that are not orthologous to the better-studied emodin/endocrocin nrPKSs of Ascomycetes, and show a distinct domain composition [19]. Here, we show that the next steps in the pathway, i.e., the *O*-methylation of the emodin and endocrocin scaffolds, also utilize enzymes that, although sharing the generalized OMT fold, are not orthologous to the AQ OMTs of Ascomycetes, even

if they share the same substrate (emodin) and afford the same product (physcion) [10, 11]. We also provide the first example, to the best of our knowledge, for an OMT that specifically recognizes endocrocin as its substrate to produce the characteristic *Cortinarius* AQ metabolite dermolutein. Thus, both AQ scaffold biosynthesis, and *O*-methylation of these scaffolds appears to have originated by parallel evolution in *Cortinarius* spp. vs. Ascomycetes.

To afford the AQ pigment assemblage typical of *Cortinarius* mushrooms, nature elected a strategy that economizes by producing two biogenically related AQ scaffolds, emodin and endocrocin, using a single nrPKS enzyme. However, these branch products are channeled towards distinct AQ pigments by separate OMT enzymes that seem to be fine-tuned to differentiate emodin and endocrocin as their respective substrates and methylate these substrates with high regioselectivity. For this task, *Cortinarius* mushrooms recruited distinct OMTs that show only moderate mutual sequence similarity (e.g., CkOMT2 and CkOMT4 show only 40% identity), instead of relying on the functional diversification of paralogs originating from a recent gene duplication.

Perhaps related, the genes for the AQ biosynthetic pathways in *Cortinarius* mushrooms are distributed into several biosynthetic gene clusters (BGCs). These BGCs are anchored by nrPKS paralogues that must have originated from (repeated) gene duplications followed by functional diversification, preserving one nrPKS for emodin and endocrocin production. Yet, in *C. sp.* KIS-3, the emodin/endocrocin-producing nrPKS CkPKS3, the physcion-producing CkOMT4, and the dermolutein-producing CkOMT2 all reside in distinct BGCs. While CsPKS2 and the dermolutein-producing CsOMT5 are clustered in *C. semisanguineus*, the other OMT encoded in that cluster (CsOMT6) does not afford physcion. Thus, the *C. semisanguineus* OMT for physcion production must reside in yet another genomic locus that, for now, remains to be identified. In any case, the patchwork nature of these biosynthetic pathways in Basidiomycetes suggests two interesting and perhaps interrelated possibilities, as already seen in a few cases in Ascomycetes [28–30]. First, coherent biosynthetic pathways may be encoded by genes that reside at distinct genomic loci and may even appear to be part of a different BGC. Second, efficient metabolic crosstalk may arise among separate BGCs encoding promiscuous enzymes: such enzymes may accomplish dedicated tasks in the pathway encoded by their “home” BGC while also “moonlighting” in different biosynthetic pathways.

Deciphering the biosynthesis of the characteristic *Cortinarius* AQs will allow the reconstruction of these pathways in efficient synthetic biology chassis that would

also make the economical production of selected congeners possible for specific applications. This will also open these AQ scaffolds for combinatorial biosynthetic modifications to adapt these interesting pigments even better for their potential uses as industrial dyes, cosmetics ingredients, photosensitizers, crop protection agents, and pharmaceuticals.

## Materials and methods

### Genome and transcriptome sequencing of *C. semisanguineus*

A pure culture of *C. semisanguineus* F-YF12 was obtained from the Luke Natural Resources Institute of Finland. The mycelium was grown at 20 °C on plates with a cellophane film on top of a modified Melin–Norkrans agar medium with reduced sugar content (½MMN: 1.25 g/L glucose, 5 g/L malt extract, 0.25 g/L (NH<sub>4</sub>)<sub>2</sub>HPO<sub>4</sub>, 0.5 g/L KH<sub>2</sub>PO<sub>4</sub>, 0.15 g/L MgSO<sub>4</sub>×7H<sub>2</sub>O, 0.05 g/L CaCl<sub>2</sub>×2H<sub>2</sub>O, 0.025 g/L NaCl, 20.16 mg/L Fe-EDTA, 10 mg/L thiamine-HCl and 18 g/L agar; pH 5.5). The mycelium was collected, frozen, and ground in liquid nitrogen. Genomic DNA was isolated with QIAGEN Genomic-tip 500/G columns according to the manufacturer’s protocol, followed by twice-repeated extractions first with phenol–chloroform–isoamyl alcohol (25:24:1, v/v), then with chloroform–isoamyl alcohol (24:1, v/v). After precipitation with isopropanol and washing with 70% ethanol, the dry DNA precipitate was dissolved in 10 mM Tris–HCl pH 8.0.

For RNA isolation, *C. semisanguineus* F-YF12 was grown as static liquid surface pure cultures at 20 °C, in 50 mL of ½MMN liquid medium in 250-ml Erlenmeyer flasks. Fungal fruiting bodies were collected from a pine forest at Southern Finland and stored at –20 °C before RNA extraction from the cap and separately, the stipe tissues. Two parallel samples each from the cap, the stipe, and the pure culture were ground in liquid nitrogen and the total RNA was extracted with a Qiagen RNeasy Mini Kit, according to the manufacturer’s protocol. RNA samples in RNase-free water were sent to Novogene (UK) for genome sequencing. After quality check, cDNA libraries were prepared with poly-A enrichment of the mRNA, and sequenced using the Illumina NovaSeq PE150 platform, resulting in 6 Gb of raw data (20 million reads) per sample.

The *Cortinarius semisanguineus* genome sequence (pure culture) was obtained using a combination of paired-end short-read sequencing (using Illumina NovaSeq 6000 platform—PE 150) and long-read sequencing approaches (using PacBio Sequel platform). RNA-sequencing of the pure cultures, caps and stipes were performed using Illumina NovaSeq 6000 platform—PE 150 in duplicates (i.e., two biological replicates each). Genome and transcriptome sequencing

and quality-filtering of the sequencing reads were performed by Novogene Europe Ltd. Because of the very high repeat content of the genome, only 2.8 Gb of high-quality nonrepetitive reads could be obtained even after 10 Gb of genome sequencing.

To obtain the genome assembly of *Cortinarius semisanguineus*, the PacBio data were converted from BAM to FASTQ format using PacBio-SMRTLink software (v9.0.0.92188) and a hybrid (i.e., long-read and short-read), de novo assembly was performed using wengan (v0.2) [31]. For a de novo gene prediction from the genome assembly, the RNA-sequencing reads, and protein sequences from the *Cortinarius* sp. KIS3-TL2766 1.0 genome dataset at the JGI portal (JGI Project ID: 1193782, [https://mycocosm.jgi.doe.gov/CorKIS3\\_1/CorKIS3\\_1.home.html](https://mycocosm.jgi.doe.gov/CorKIS3_1/CorKIS3_1.home.html)) and the fungal proteins dataset from OrthoDB (v10) [32] were used. The gene prediction was performed using the BRAKER2 workflow with RNA-seq data and protein data separately and using TSEBRA for combining the two gene prediction results [33, 34].

The RNA-sequencing reads of the six samples were pooled and assembled de novo using trinity [35], and functionally annotated with Trinotate, Transdecoder [35] and Egnog [36]. The gene expression in the six samples was quantified using Kallisto [37] and normalized using Trimmed Mean of M-values (TMM) for differential expression analysis with EdgeR [38].

### Phylogenetic analysis and docking

Multiple sequence alignments were built using MUSCLE, implemented in Geneious Prime 2023.0.4 ([www.geneious.com](http://www.geneious.com)). Phylogenetic trees were constructed with the neighbor-joining method using the Jukes-Cantor genetic distance model, with bootstrapping set to 1000 replicates. The trees were visualized with Geneious Prime 2023.0.4.

Protein structure models were constructed using AlphaFold 2 [39]. Protein, co-product (SAH), and substrate structures were refined using AutoDock tools [40] (<https://ccsb.scripps.edu/mgltools/-1-5-6/>), and docking was performed using AutoDock Vina [41] following a two-step consecutive approach (the SAH co-product was docked first to the enzyme, and the best docking pose was used for a second round of docking with the substrate). The best docking poses in each case were selected based on the low affinity score (higher binding affinity), followed by comparing the orientations of these ligands with those in the available crystal structure of GedA (PDB id: 7WH9). The visualization and analysis of the docked poses were performed using Pymol version 2.5.5 ([www.pymol.org](http://www.pymol.org)).

### Construction of *S. cerevisiae* plasmids

All *S. cerevisiae* plasmids (SI Table S17) were constructed using Gibson assembly (Gibson Assembly Mastermix, NEB) unless mentioned otherwise, and validated by sequencing. The codon-optimized phosphopantetheinyl transferase gene *npgA* of *Aspergillus nidulans* (GenBank: XP\_663744) was custom-synthesized (Integrated DNA Technologies, USA), and amplified by PCR using the appropriate primers (SI Table S18). The *acc1\*\** gene fragment was obtained by digesting plasmid pSK293 (SI Table S17) with *NotI*, *SacI*, and *PvuI*. These two genes, along with the SES bi-directional promoter [22] were assembled into the *MluI*-digested pB13472 vector that included targeting arms to the *S. cerevisiae* *LEU* locus, to afford pB13474.

Genes for CsPKS1, CkPKS3, CkPKS4, and those for all the OMTs were obtained as synthetic gene blocks (Integrated DNA Technologies, USA) codon optimized for *Aspergillus niger*. CsPKS2 and CkPKS5 could not be synthesized by the supplier. The intron-free open reading frame encoding CsPKS2 was then amplified by RT-PCR using *C. semisanguineus* cDNA from the cap as the template. Expression cassettes with the SES promoter [22] were constructed for the PKS-encoding genes, with or without any one of the genes for the OMTs, with genome integration targeting arms to the *S. cerevisiae* *HIS* locus. Expression cassettes for CkOMT4 and CsOMT5 were constructed by digesting pB13482 and pB13483, respectively, with *PacI* and *XhoI* to release the PKS-encoding fragments, filling the overhanging base pairs with Klenow polymerase, and re-circularizing the plasmid to obtain pB14444 and pB14445. All the protein sequences are listed in SI Table S19.

### Construction of *S. cerevisiae* strains

To construct the *S. cerevisiae* H6108 chassis with the genes encoding *NpgA* and *ACC1\*\** (SI Table S10), the plasmid pB13474 (SI Table S17) was digested with *NotI* and the integration cassette was transformed into *S. cerevisiae* H4590 using the lithium acetate and PEG-mediated transformation protocol as described [42]. The transformed cells were plated on SC-LEU selection plates and validated for the correct genomic integration into the *leu2-3* locus using qPCR.

The resulting *S. cerevisiae* H6108 strain was used as the chassis strain for all the other constructs. Thus, this strain was transformed separately with the CsPKS1, CsPKS2, CkPKS3, or CkPKS4 expression cassettes, released from the pB13476, pB14914, pB13477, and pB13478 plasmids (SI Table S17), respectively, by *NotI* digestion. Similarly, H6108 strain was transformed with the bi-directional expression cassettes co-expressing CkPKS3 with the

individual OMTs, released from the pB13479-pB13484 plasmids (SI Table S17), respectively, by *NotI* digestion. The transformants were selected on SC-HIS agar plates, and validated for the presence of the expression cassette and the deletion of the *his3-Δ1* locus using qPCR.

#### Strain cultivation and sample preparation

For total biosynthesis, three independent, verified *S. cerevisiae* H6108 transformants for each strain were cultivated in 4 mL TSB (17 g/L tryptone, 3 g/L soytone, 5 g/L NaCl, 2.5 g/L  $K_2HPO_4$ ; pH 7.3) + 2% glucose medium in 24-well plates at 28 °C for 72 h with shaking at 800 rpm. For in vivo biocatalytic transformation, three to five independent, verified *S. cerevisiae* H6108 transformants were cultivated in 25 mL of SD-dropout medium at 30 °C with shaking at 200 rpm until the cultures reached an optical density at 600 nm ( $OD_{600}$ ) of 1.0. These precultures were then used for inoculating 25 mL TSB media with 2% glucose in shake flasks and the cultures were incubated at 30 °C with shaking at 200 rpm for 6 h. The substrate (dissolved in ethanol) was supplemented at the final concentration of 25 mg/L, and cultivation was continued at 30 °C with shaking at 200 rpm for 3 days.

The cultures were then centrifuged, and the supernatants were analyzed directly by LC-MS. The cells were extracted with 1 mL methanol at 37 °C with shaking at 240 rpm for 1 h, centrifuged at 4000 rpm for 5 min, the supernatants were collected, and analyzed by LC-MS. Cultivation experiments were repeated at least three times for quantification. Fermentations were scaled up for the isolation of AQs to two to five liters, depending on yield. The cultures were extracted with ethyl acetate (EtOAc), the organic fractions were dried under reduced pressure at 50 °C and dissolved in methanol.

#### Protein expression and purification

*S. cerevisiae* H6111 was transformed with yeast 2 $\mu$ -based plasmids harboring genes for the N- or C-terminally His<sub>6</sub>-tagged CkOMT4 or CsOMT5 (SI Tables S10 and S17), and the activity of the His<sub>6</sub>-tagged OMTs were confirmed by verifying the in vivo biocatalytic production of the O-methylated AQs before proceeding with enzyme purification. A negative control strain was also constructed by transforming strain H6111 with the empty vector (pB14913). The strains producing the N-terminally His<sub>6</sub>-tagged OMTs were then grown in 400 mL YPD medium supplemented with 200  $\mu$ g/mL (final concentration) nourseothricin in 2.5-L Erlenmeyer flasks at 30 °C with shaking at 200 rpm for 2 days. The cells were harvested by centrifugation at 4000 rpm for 10 min and resuspended in 50 mL of ice-cold lysis buffer (20 mM sodium phosphate, 0.5 M NaCl, 5 mM imidazole, pH 7.4), supplemented with protease inhibitors (1 $\times$ Complete,

EDTA-free Protease Inhibitor Cocktail, Roche). The cell suspensions were combined with 0.5 mm dia. glass beads (Biospec) and lysed using a BeadBeater (Biospec). The extent of the lysis was monitored using a microscope. The lysate was centrifuged at 27,000g for 45 min at 4 °C, and the supernatant was loaded onto a 1 mL HiTrap Chelating HP column equilibrated with Binding buffer (20 mM sodium phosphate, 0.5 M NaCl, 5 mM imidazole, pH 7.4). The recombinant OMT enzymes were eluted with a 10 mL gradient of imidazole (0–500 mM), and the fractions were analyzed by SDS-PAGE. Fractions having the target OMTs were pooled and used for in vitro assays.

#### In vitro assay conditions

Enzyme activity assays were performed in 100  $\mu$ L reaction mixtures containing 20 mM Tris-HCl pH 7.5, 10% glycerol, 100  $\mu$ M substrate, and 1 mM S-adenosyl methionine (SAM) as the methyl group donor. Reactions were initiated by adding the OMT enzyme and the mixtures were incubated for 1 h (for native substrates) or overnight (for substrate analogues) at 30 °C. The reactions were quenched by adding an equal amount of methanol. The samples were then centrifuged at 13,500 rpm for 15 min and analyzed by HPLC.

#### Purification and structure elucidation of physcion (4) and dermolutein (5)

For producing physcion (4), the *S. cerevisiae* H6108 strain expressing CkOMT4 was cultivated in 50 mL YPD medium at 30 °C with shaking at 200 rpm until the culture reached  $OD_{600}$  of 2.0. The cells were harvested by centrifugation at 4000 rpm for 5 min, and used to inoculate 50 mL fresh TSB medium with 2% glucose (supplemented with 10 mg of substrate). For producing dermolutein 5, the H6108-derived strain expressing CsOMT5 and CkPKS3 was used for de novo biosynthesis in large-scale cultivations in TSB media (2% glucose). The cultures were incubated at 30 °C with shaking at 200 rpm for 72 h and extracted twice with an equal volume of EtOAc. The organic fractions were collected, dried first using a Heidolph Rotary evaporator (Schwabach, Germany) at reduced pressure, followed by drying under N<sub>2</sub> flow in a TurboVap evaporator (Caliper Life Sciences, Massachusetts). The residue was resuspended in methanol and subjected to reversed-phase C18 silica gel column chromatography (25 g), eluted with an acetonitrile/water gradient. The fractions were analyzed by LC-MS, and those containing the target compounds were further purified by preparative HPLC on a Waters Alliance system with a DAD detector, equipped with a SunFire prep C18 OBD reversed-phase column (5  $\mu$ m, 19 mm $\times$ 100 mm). NMR experiments were carried out at 25 °C on a 600 MHz Bruker Avance III NMR spectrometer equipped

with a QCI H-P/C/N-D cryoprobe. 1D  $^1\text{H}$  and  $^{13}\text{C}$  spectra were obtained using the standard pulse sequences. The  $^1\text{H}$  couplings were removed from the  $^{13}\text{C}$  spectra by inverse gated waltz-16 decoupling. 2D NMR (HSQC, HMBC, and  $^1\text{H}$ - $^1\text{H}$  COSY) spectra were obtained using standard Bruker pulse programs hsqcedetgpsisp2.2, hmbcgpplndqf and cosygpprqf, respectively. In HMBC, the long-range evaluation delay was optimized for 8 Hz (62.5 ms). Chemical shift values ( $\delta$ ) are given in parts per million (ppm), and the coupling constants ( $J$  values) are in Hz. All spectra were recorded in DMSO- $d_6$ , 99.8% D (Eurisotop, St-Aubin Cedex, France) and the chemical shifts were referenced to the residual  $^1\text{H}$  and  $^{13}\text{C}$  solvent signals at 2.5 and 39.52 ppm, respectively.

### LC–MS analysis

LC–MS analysis was performed on an Acquity UHPLC system equipped with a Synapt G2-S MS detector (both Waters, USA), using an Acquity UPLC BEH HSS T3 column (1.8  $\mu\text{m}$  2.1  $\times$  100 mm, kept at 45  $^\circ\text{C}$ ), at a flow rate of 0.4 mL/min with mobile phase A (0.1% formic acid in water) and B (0.1% formic acid in acetonitrile). The gradient elution started at 5% B maintained for 0.2 min, then increased to 90% B in 14 min, then directly returned to 5% B and was maintained for 3 min. Mass spectrometry was carried out by electrospray ionization (ESI) in negative polarity using a capillary voltage of 2.0 kV and cone voltage of 40 kV. The source temperature was 150  $^\circ\text{C}$  and the desolvation temperature was 500  $^\circ\text{C}$ . The desolvation gas flow was set at 800 L/h (nitrogen). The percentage errors in masses measured by LC–MS/MS are listed in SI Table S20.

### Supplementary Information

The online version contains supplementary material available at <https://doi.org/10.1186/s13068-025-02625-6>.

Supplementary Material 1

### Acknowledgements

We thank Esa Tanhola and Walteri Hosia for their help with preparative HPLC and Sanna Haasiosalo and Iita Ollanketo for preparing the media. We would also like to thank Taina Pennanen (Natural Resources Institute Finland [Luke]) for providing the pure culture of *C. semisanguineus* F-YF12 and to Riikka Räsänen (University of Helsinki) for providing the *C. semisanguineus* fruiting bodies for RNA isolation.

### Author contributions

P.J., D.M., and I.M. designed the experiments; P.J. conducted most of the experiments together with contribution from S.H., J.R., N.M., and H.M.; G.P. assembled the sequencing data; P.J. and S.C. performed the docking studies; M.P., I.M., M.T., and D.M. conceived, supervised, and coordinated the study. P.J. and I.M. drafted the manuscript; All authors read and approved the final manuscript.

### Funding

This research was supported by the Jenny and Antti Wihuri Foundation (Center for Young Synbio Scientists to M.P.), the Strategic Research Council

(STN) of the Research Council of Finland (BioColour project, Funding no. 327193 to M.P.), and the Research Council of Finland (Grant Number 361876 to I.M.).

### Data availability

Protein sequences are submitted to GenBank. Data is provided within the manuscript or supplementary information files.

### Declarations

#### Ethics approval and consent to participate

Not applicable.

#### Competing interests

The OMT enzymes presented here are the subjects of PC22105FI / P5120FI00, assigned to VTT Technical Research Centre of Finland. The authors declare no other conflicts of interest.

Received: 6 September 2024 Accepted: 15 February 2025

Published online: 25 February 2025

### References

- Abdelraheem E, Thair B, Varela RF, Jockmann E, Popadić D, Hailles HC, Ward JM, Iribarren AM, Lewkowicz ES, Andexer JN, Hagedoorn PL, Hanefeld U. Methyltransferases: functions and applications. *ChemBioChem*. 2022;23(18):1–19. <https://doi.org/10.1002/cbic.202200212>.
- Xue Y, Liang Y, Zhang W, Geng C, Feng D, Huang X, Dong S, Zhang Y, Sun J, Qi F, Lu X. Characterization and structural analysis of Emodin-O-methyltransferase from *Aspergillus terreus*. *J Agric Food Chem*. 2022;70:5728–37. <https://doi.org/10.1021/acs.jafc.2c01281>.
- Wang X, Wang C, Duan L, Zhang L, Liu H, Xu YM, Liu Q, Mao T, Zhang W, Chen M, Lin M, Gunatilaka AAL, Xu Y, Molnár I. Rational reprogramming of O-methylation regioselectivity for combinatorial biosynthetic tailoring of benzenediol lactone scaffolds. *J Am Chem Soc*. 2019;141(10):4355–64. <https://doi.org/10.1021/jacs.8b12967>.
- Suthar M, Lagashetti AC, Räsänen R, Singh PN, Dufossé L, Robinson SC, Singh SK. Industrial applications of pigments from macrofungi. In: Press CRC, editor. *Advances in macrofungi*. New York: CRC Press; 2021. p. 223–51. <https://doi.org/10.1201/9781003096818-17>.
- Zalas M, Gierczyk B, Bogacki H, Schroeder G. The *Cortinarius* fungi dyes as sensitizers in dye-sensitized solar cells. *Int J Photoenergy*. 2015;2015:653740. <https://doi.org/10.1155/2015/653740>.
- de Mattos-Shiple KJ, Simpson TJ. The 'Emodin Family' of fungal natural products amalgamating a century of research with recent genomics-based advances. *Nat Prod Rep*. 2023;40:174–201. <https://doi.org/10.1039/d2np00040g>.
- Pang MJ, Yang Z, Zhang XL, Liu ZF, Fan J, Zhang HY. Physcion, a naturally occurring anthraquinone derivative, induces apoptosis and autophagy in human nasopharyngeal carcinoma. *Acta Pharmacol Sin*. 2016;37(12):1623–40. <https://doi.org/10.1038/aps.2016.98>.
- Yang X, Yang L, Ni H, Yu D. Effects of physcion, a natural anthraquinone derivative, on the infection process of *Blumeria graminis* on wheat. *Can J Plant Pathol*. 2008;30(3):391–6. <https://doi.org/10.1080/0706060809507536>.
- Li J, Han A, Zhang L, Meng Y, Xu L, Ma F, Liu R. Chitosan oligosaccharide alleviates the growth inhibition caused by physcion and synergistically enhances resilience in maize seedlings. *Sci Rep*. 2022;12(1):162. <https://doi.org/10.1038/s41598-021-04153-3>.
- Qi F, Zhang W, Xue Y, Geng C, Jin Z, Li J, Guo Q, Huang X, Lu X. Microbial production of the plant-derived fungicide physcion. *Metab Eng*. 2022;74:130–8. <https://doi.org/10.1016/j.ymben.2022.10.007>.
- Yao Y, Yang EL, Pan Y, Shu X, Liu G. Mining an O-methyltransferase for de novo biosynthesis of physcion in *Aspergillus nidulans*. *Appl Microbiol Biotechnol*. 2023;107(4):1177–88. <https://doi.org/10.1007/s00253-023-12373-y>.

12. Guo L, Zhang F, Wang X, Chen H, Wang Q, Guo J, Cao X, Wang L. Antibacterial activity and action mechanism of questin from marine *Aspergillus flavipes* HN4–13 against aquatic pathogen vibrio harveyi. *3 Biotech*. 2019;9(1):14. <https://doi.org/10.1007/s13205-018-1535-1>.
13. Siewert B, Ćurak G, Hammerle F, Huymann L, Fiala J, Peintner U. The photosensitizer emodin is concentrated in the gills of the fungus *Cortinarius rubrophyllus*. *J Photochem Photobiol B*. 2022;228:112390. <https://doi.org/10.1016/j.jphotobiol.2022.112390>.
14. Räsänen R. Fungal colorants in applications—focus on *Cortinarius* species. *Color Technol*. 2019;135(1):22–31. <https://doi.org/10.1111/cote.12376>.
15. Jean G, Chantal F. Two-stage process for dyeing keratin fibres. 1984. US Patent US4566875A
16. Räsänen R, Primetta A, Nikunen S, Honkalampi U, Nygren H, Pihlava JM, Vanden Bl, von Wright A. Examining safety of biocolourants from fungal and plant sources—examples from *Cortinarius* and *Tapinella*, *Salix* and *Tanacetum* Spp. and dyed woollen fabrics. *Antibiotics*. 2020;9(5):266. <https://doi.org/10.3390/antibiotics9050266>.
17. Herrala M, Yli-Öyrä J, de Albuquerque AF, de Farias NO, Moraes DA, Räsänen R, Freeman HS, Umbuzeiro GA, Rysä J. Waterless dyeing and in vitro toxicological properties of biocolourants from *Cortinarius sanguineus*. *J Fungus*. 2022;8(11):1129. <https://doi.org/10.3390/jof8111129>.
18. Löhr NA, Eisen F, Thiele W, Platz L, Motter J, Hüttel W, Gressler M, Müller M, Hoffmeister D. Unprecedented mushroom polyketide synthases produce the universal anthraquinone precursor. *Angew Chem Int Ed*. 2022;61(24):e202116142. <https://doi.org/10.1002/anie.202116142>.
19. Löhr NA, Rakhmanov M, Wurlitzer JM, Lackner G, Gressler M, Hoffmeister D. Basidiomycete non-reducing polyketide synthases function independently of SAT domains. *Fungal Biol Biotechnol*. 2023;10(1):17. <https://doi.org/10.1186/s40694-023-00164-z>.
20. Keszenman-Pereyra D, Lawrence S, Twifeg ME, Price J, Turner G. The NpgA/CfwA gene encodes a putative 4'-phosphopantetheinyl transferase which is essential for penicillin biosynthesis in *Aspergillus nidulans*. *Curr Genet*. 2003;43(3):186–90. <https://doi.org/10.1007/s00294-003-0382-7>.
21. Pedersen TB, Nielsen MR, Kristensen SB, Spedtsberg EML, Sørensen T, Petersen C, Muff J, Sondergaard TE, Nielsen KL, Wimmer R, Gardiner DM, Sørensen JL. Speed dating for enzymes! Finding the perfect phosphopantetheinyl transferase partner for your polyketide synthase. *Microb Cell Fact*. 2022;21(1):1–10. <https://doi.org/10.1186/s12934-021-01734-9>.
22. Rantasalo A, Landowski CP, Kuivanen J, Korppoo A, Reuter L, Koivistoinen O, Valkonen M, Penttilä M, Jääntti J, Mojitá D. A universal gene expression system for fungi. *Nucleic Acids Res*. 2018;46(18):e111. <https://doi.org/10.1093/nar/gky558>.
23. Choi JS, Jung JH, Lee HJ, Kang SS. The NMR assignments of anthraquinones from *Cassia tora*. *Arch Pharm Res*. 1996;19(4):302–6. <https://doi.org/10.1007/BF02976245>.
24. Joshi CP, Chiang VL. Conserved sequence motifs in plant S-Adenosyl-L-methionine-dependent methyltransferases. *Plant Mol Biol*. 1998;37:663–74. <https://doi.org/10.1023/A:1006035210889>.
25. Bond CM, Tang Y. Engineering *Saccharomyces cerevisiae* for production of simvastatin. *Metab Eng*. 2019;51(1):1–8. <https://doi.org/10.1016/j.ymben.2018.09.005>.
26. Hannecker A, Huymann L, Hammerle F, Peintner U, Siewert B. Photochemical defense as trait of fungi from *Cortinarius* subgenus dermocybe. *Photochem Photobiol Sci*. 2023;22(1):147–57. <https://doi.org/10.1007/s43630-022-00305-0>.
27. Hammerle F, Fiala J, Höck A, Huymann L, Vrabl P, Husiev Y, Bonnet S, Peintner U, Siewert B. Fungal anthraquinone photoantimicrobials challenge the dogma of cationic photosensitizers. *J Nat Prod*. 2023;86(10):2247–57. <https://doi.org/10.1021/acs.jnatprod.2c01157>.
28. Bradshaw RE, Slot JC, Moore GG, Chettri P, de Wit PJGM, Ehrlich KC, Ganley ARD, Olson MA, Rokas A, Carbone I, Cox MP. Fragmentation of an aflatoxin-like gene cluster in a forest pathogen. *New Phytol*. 2013;198(2):525–35. <https://doi.org/10.1111/nph.12161>.
29. Schumacher J. DHN melanin biosynthesis in the plant pathogenic fungus *Botrytis cinerea* is based on two developmentally regulated key enzyme (PKS)-encoding Genes. *Mol Microbiol*. 2016;99(4):729–48. <https://doi.org/10.1111/mmi.13262>.
30. Araki Y, Awakawa T, Matsuzaki M, Cho R, Matsuda Y, Hoshino S, Shinohara Y, Yamamoto M, Kido Y, Inaoka DK, Nagamune K, Ito K, Abe I, Kita K. Complete biosynthetic pathways of ascofuranone and ascochlorin in *Acremonium egypiticum*. *Proc Natl Acad Sci USA*. 2019;116(17):8269–74. <https://doi.org/10.1073/pnas.1819254116>.
31. Di Genova A, Buena-Atienza E, Ossowski S, Sagot M-F. Efficient hybrid de novo assembly of human genomes with WENGAN. *Nat Biotechnol*. 2021;39(4):422–30. <https://doi.org/10.1038/s41587-020-00747-w>.
32. Kriventseva EV, Kuznetsov D, Tegenfeldt F, Manni M, Dias R, Simão FA, Zdobnov EM. OrthoDB V10: sampling the diversity of animal, plant, fungal, protist, bacterial and viral genomes for evolutionary and functional annotations of orthologs. *Nucleic Acids Res*. 2019;47(D1):D807–11. <https://doi.org/10.1093/nar/gky1053>.
33. Brůna T, Hoff KJ, Lomsadze A, Stanke M, Borodovsky M. BRAKER2: automatic eukaryotic genome annotation with GeneMark-EP+ and AUGUSTUS supported by a protein database. *NAR Genom Bioinform*. 2021;3(1):1–11. <https://doi.org/10.1093/NARGAB/LQAA108>.
34. Gabriel L, Hoff KJ, Brůna T, Borodovsky M, Stanke M. TSEBRA: transcript selector for BRAKER. *BMC Bioinformatics*. 2021;22(1):1–12. <https://doi.org/10.1186/S12859-021-04482-0>.
35. Grabherr MG, Haas BJ, Yassour M, Levin JZ, Thompson DA, Amit I, Adiconis X, Fan L, Raychowdhury R, Zeng Q, Chen Z, Mucelli E, Hacohen N, Gnirke A, Rhind N, Di Palma F, Birren BW, Nusbaum C, Lindblad-Toh K, Friedman N, Regev A. Full-length transcriptome assembly from RNA-Seq data without a reference genome. *Nat Biotechnol*. 2011;29(7):644–52. <https://doi.org/10.1038/nbt.1883>.
36. Huerta-Cepas J, Szklarczyk D, Heller D, Hernández-Plaza A, Forslund SK, Cook H, Mende DR, Letunic I, Rattei T, Jensen LJ, Von Mering C, Bork P. EggNOG 5.0: a hierarchical, functionally and phylogenetically annotated orthology resource based on 5090 organisms and 2502 viruses. *Nucleic Acids Res*. 2019;47(D1):D309–14. <https://doi.org/10.1093/nar/gky1085>.
37. Bray NL, Pimentel H, Melsted P, Pachter L. Near-optimal probabilistic RNA-Seq quantification. *Nat Biotechnol*. 2016;34(5):525–7. <https://doi.org/10.1038/nbt.3519>.
38. McCarthy DJ, Chen Y, Smyth GK. Differential expression analysis of multi-factor RNA-Seq experiments with respect to biological variation. *Nucleic Acids Res*. 2012;40(10):4288–97. <https://doi.org/10.1093/NAR/GKS042>.
39. Mirdita M, Schütze K, Moriwaki Y, Heo L, Ovchinnikov S, Steinegger M. ColabFold: making protein folding accessible to all. *Nat Methods*. 2022;19(6):679–82. <https://doi.org/10.1038/s41592-022-01488-1>.
40. Forli S, Huey R, Pique ME, Sanner MF, Goodsell DS, Olson AJ. Computational protein-ligand docking and virtual drug screening with the AutoDock suite. *Nat Protoc*. 2016;11(5):905–19. <https://doi.org/10.1038/nprot.2016.051>.
41. Eberhardt J, Santos-Martins D, Tillack AF, Forli S. AutoDock Vina 1.2.0: new docking methods, expanded force field, and Python bindings. *J Chem Inf Model*. 2021;61(8):3891–8. <https://doi.org/10.1021/acs.jcim.1c00203>.
42. Gietz RD. Yeast transformation by the LiAc/SS carrier DNA/PEG method. *Methods Mol Biol*. 2014;2014:1205. [https://doi.org/10.1007/978-1-4939-1363-3\\_1](https://doi.org/10.1007/978-1-4939-1363-3_1).

## Publisher's Note

Springer Nature remains neutral with regard to jurisdictional claims in published maps and institutional affiliations.